HHS Public Access

Author manuscript

J Biomed Mater Res A. Author manuscript; available in PMC 2016 October 01.

Published in final edited form as:

J Biomed Mater Res A. 2015 October ; 103(10): 3407–3418. doi:10.1002/jbm.a.35445.

Immobilized Surfactant-Nanotube Complexes Support Selectin-Mediated Capture of Viable Circulating Tumor Cells in the Absence of Capture Antibodies

Michael J. Mitchell[1,2], **Carlos A. Castellanos**[1], and **Michael R. King**[1,*]

[1]Department of Biomedical Engineering, Cornell University, Ithaca, NY 14853, USA

[2]David H. Koch Institute for Integrative Cancer Research, Department of Chemical Engineering, Massachusetts Institute of Technology, Cambridge, MA 02139, USA

Abstract

The metastatic spread of tumor cells from the primary site to anatomically distant organs leads to a poor patient prognosis. Increasing evidence has linked adhesive interactions between circulating tumor cells (CTCs) and endothelial cells to metastatic dissemination. Microscale biomimetic flow devices hold promise as a diagnostic tool to isolate CTCs and develop metastatic therapies, utilizing E-selectin (ES) to trigger the initial rolling adhesion of tumor cells under flow. To trigger firm adhesion and capture under flow, such devices also typically require antibodies against biomarkers thought to be expressed on CTCs. This approach is challenged by the fact that CTCs are now known to exhibit heterogeneous expression of conventional biomarkers. Here, we describe surfactant-nanotube complexes to enhance ES-mediated capture and isolation of tumor cells without the use of capture antibodies. While the majority of tumor cells exhibited weaker rolling adhesion on halloysite nanotubes (HNT) coated with ES, HNT functionalization with the sodium dodecanoate (NaL) surfactant induced a switch to firm cellular adhesion under flow. Conversely, surfactant-nanotube complexes significantly reduced the number of primary human leukocytes captured via ES-mediated adhesion under flow. The switch in tumor cell adhesion was exploited to capture and isolate tumor cells in the absence of EpCAM antibodies, commonly utilized as the gold standard for CTC isolation. Additionally, HNT-NaL complexes were shown to capture tumor cells with low to negligible EpCAM expression, that are not efficiently captured using conventional approaches.

Keywords

Nanotube; Circulating Tumor Cell; Metastasis; Biomaterials; Cancer

INTRODUCTION

Metastasis is the primary cause of over 90% of cancer-related deaths[(1)]. During metastasis, as many as one million tumor cells per gram of tumor per day[(2),(3)] are shed from the primary tumor site, and enter the circulation as circulating tumor cells (CTCs) via

* Correspondence: mike.king@cornell.edu.

intravasation[4],[5]. CTCs must survive hemodynamic shear forces and immunological stress to translocate through the bloodstream to microvessels in anatomically distant organs [6],[7]. In the microvasculature, CTCs adhesively interact with the receptor-bearing endothelial cell wall, in a manner similar to the leukocyte adhesion cascade during inflammation [8],[9]. Recent studies have shown that, similar to leukocytes, glycosylated ligands are expressed on the CTC surface, which trigger the initial adhesion with selectin receptors on the endothelium[10],[11]. The rapid, force-dependent binding kinetics of selectins initiate CTC rolling adhesion along the blood vessel wall[12],[13]. CTCs then transition from rolling to firm adhesion, allowing for transmigration into tissues and the formation of secondary tumors[14]. Surgery, radiation, and chemotherapy are generally successful at treating primary tumors that do not invade the basement membrane, however the difficulty of detecting and treating metastases in anatomically distant organs leads to a poor patient prognosis. Because of this, several approaches are being developed to isolate CTCs from the bloodstream for use in personalized medicine regimens [15]-[17], and also to target and kill CTCs in the bloodstream before the formation of metastases [18]-[22].

The separation of viable CTCs in relatively large quantities and high purity levels from patient blood could lead to the development of effective personalized medicine regimens for those with metastatic cancer[23]. However, CTCs are sparsely distributed in the bloodstream, at concentrations as low as 1-100 cells/mL[24]. The separation and isolation of CTCs from blood is commonly referred to as a “needle in a haystack problem”, as leukocytes and erythrocytes are present in concentrations of one million and one billion cells per mL of blood, respectively[25],[26]. Thus, numerous techniques for tumor cell isolation have been developed, including magnetic bead-based cell isolation [27], flow-based microfluidic platforms [15],[28], and technologies to isolate tumor cells based on chemotactic phenotype [29]. The only FDA-approved CTC isolation system, CellSearch®, separates CTCs from blood using magnetic beads coated with anti-epithelial cell adhesion molecule (EpCAM) antibodies [24]. However, CTCs do not remain viable after CellSearch® isolation, which is essential for individualized disease prognosis and *in vitro* testing of therapeutics on a patient-to-patient basis. Our lab has recently developed microscale flow devices that mimic the metastatic adhesion cascade process to capture and separate CTCs from whole blood under flow conditions. The device consists of a biomaterial surface coated with recombinant human E-selectin (ES), which triggers the initial rolling adhesion of tumor cells, and capture antibodies against the CTC markers EpCAM or prostate-specific membrane antigen (PSMA), which firmly adhere and capture tumor cells from flow. These flow devices have been shown to rapidly separate viable CTCs from patient blood, which then remain viable in culture [15]. Such devices have also been used to enumerate CTCs after testing of therapeutics in patient blood *in vitro* as a means of developing personalized medicine regimens [30]. However, both CellSearch® and flow-based capture assays require the use of capture antibodies against specific biomarkers thought to be expressed on CTCs in order to facilitate isolation. This limits CTC isolation, given that recent work has shown CTCs to be heterogeneous in phenotype [26],[31],[32]. For example, CTCs isolated from breast cancer patients that lack EpCAM expression, and thus would not be captured using current technologies, were grown in culture and found to be capable of forming brain and

lung metastases in mice[32]. Thus, there is a need to develop CTC isolation technologies that do not require the use of capture antibodies.

Halloysite nanotubes (HNT) are naturally occurring clay minerals that have been found by our lab to promote tumor cell adhesion under flow[33]. HNT are characteristically 50-70 nm in outer diameter, and 10-30 nm in inner diameter, and 800±300 nm in length[34]. Halloysite ($Al_2Si_2O_5(OH)_4$) is a two-layered (1:1) aluminosilicate consisting of an outer siloxane (Si-O-Si) surface and an internal aluminol (Al-OH) surface[35]. HNT possesses a negatively charged outer surface and a positively charged inner lumen at physiological pH[36], and have been utilized for the encapsulation and controlled release of drugs such as Furosemide and Dexamethasome[37]. Differences in internal and external HNT charge have also been utilized for the adsorption of anionic and cationic surfactants, which significantly altered HNT zeta potential[38]. Our lab has shown that nanostructured HNT-coated biomaterials can increase surface area and selectin protein adsorption[33], which enhanced tumor cell adhesion under flow. In the present study, we explored the use of HNT and anionic surfactants to create nanostructured biomaterials consisting of surfactant-nanotube complexes to facilitate ES-mediated tumor cell capture in the absence of capture antibodies.

MATERIALS AND METHODS

Cell Culture

Human breast adenocarcinoma MCF7 (ATCC #HTB-22), colon adenocarcinoma COLO 205 (ATCC #CCL-222), lung adenocarcinoma A549 (ATCC #CCL-185) and breast carcinoma Hs 578T (ATCC #HTB-126) cell lines were purchased from American Type Culture Collection (ATCC; Manassas, VA, USA). COLO 205 cells were grown in RPMI 1640 medium supplemented with 10% fetal bovine serum (FBS) and 1% PenStrep (PS), all purchased from Invitrogen (Grand Island, NY, USA). MCF7 cells were cultured in Eagle's minimum essential medium supplemented with 0.01 mg/mL bovine insulin, 10% FBS, and 1% PenStrep, all purchased from Invitrogen. A549 cells were grown in F-12K medium supplemented with 10% FBS, and 1% PenStrep, all purchased from Invitrogen. MCF7 cells were cultured in Dulbecco's modified Eagle's medium supplemented with 0.01 mg/mL bovine insulin, 10% FBS, and 1% PenStrep, all purchased from Invitrogen. Cell lines were incubated at 37°C and 5% CO_2 under humidified conditions, and did not exceed 90% confluence. For capture assays, tumor cells were removed from culture via treatment with trypsin-EDTA (Invitrogen) for 10 min prior to handling. All cells were washed in HBSS, and resuspended at a concentration of 1.0×10^6 cells/mL in HBSS flow buffer supplemented with 0.5% HSA, 2 mM Ca^{2+}, and 10 mM HEPES (Invitrogen), buffered to pH 7.4.

Primary Human Neutrophil Isolation

Primary human neutrophils were isolated from blood as described previously[39],[40]. All human subject protocols were approved by the Institutional Review Board for Human Participants of Cornell University. Human peripheral blood was collected from healthy blood donors via venipuncture after informed consent and stored in heparin containing tubes (BD Biosciences, San Jose, CA, USA). Blood was carefully layered over 1-Step™ Polymorphs (Accurate Chemical and Scientific Corporation, Westbury, NY, USA) and

separated via centrifugation using a Marathon 8K centrifuge (Fisher Scientific, Pittsburgh, PA, USA) 480 X g for 50 min at 23°C. Neutrophils were extracted and washed in Ca^{2+} and Mg^{2+}-free HBSS, and all remaining red blood cells in the suspension were lysed hypotonically. Prior to capture assays, neutrophils were resuspended in HBSS flow buffer supplemented with 0.5% human serum albumin (HSA), 2 mM Ca^{2+}, and 10 mM HEPES (Invitrogen), buffered to pH 7.4.

Nanotube Functionalization

Halloysite nanotubes (HNT; NaturalNano, Rochester, NY, USA) were added to water at a concentration of 6.6% (w/v). 1.6 g HNT was added to 100 mL of 0.1 M aqueous sodium dodecanoate (NaL) and mixed using a magnetic stirrer at RT for 48 h (Fig. 1A). Surfactant-treated nanotubes (NaL-HNT) were then washed several times in water and allowed to dry overnight. HNT and NaL-HNT were stored in water at a concentration of 6.6% (w/v). To assess adsorption of surfactants and ES to HNT, the zeta potential (mV) of HNT and NaL-HNT, with and without ES adsorption, were measured by dynamic light scattering (DLS) using a Malvern Zetasizer Nano ZS (Malvern Instruments Ltd., Worcestershire, UK). HNT and NaL-HNT at a concentration of 0.37% (w/v) were prepared using the same solvents as described above. To assess the effect of ES adsorption on HNT and NaL-HNT zeta potential, 0.5 mL of HNT, and NaL-HNT at a concentration of 1.1% (w/v) were centrifuged at 13,000 rpm for 10 min and incubated with 0.5 mL of ES at a concentration of 2.5 μg/mL for 2.5 h at RT. Samples were centrifuged at 13,000 rpm for 10 min and resuspended in water at the same concentration used for zeta potential measurements. Colloidal stability of HNT and NaL-HNT was assessed by allowing samples to settle for 24 h post-mixing (Fig. 1B).

Fabrication of Nanostructured Biomaterial Surfaces

Microrenathane (MRE) tubing (Braintree Scientific, Braintree, MA, USA) with inner diameter 300 μm and length 55 cm was fastened onto the stage of an Olympus IX-71 inverted microscope (Olympus, Center Valley, PA, USA). 70% ethanol (v/v) was perfused through the tubes using a motorized syringe pump (KDS 230; IITC Life Science, Woodland Hills, CA, USA) at a flow rate of 1 mL/min. To functionalize the inner MRE surface with HNT, microtubes were washed thoroughly with distilled water, incubated with poly-L-lysine solution (0.02% w/v in water) for 5 min, and then coated with HNT or NaL-HNT (1.1% w/v) for 5 min (Fig. 1C). Microtubes were washed thoroughly with distilled water at 0.02 mL/min to remove unbound nanotubes, and cured overnight at room temperature (RT). To immobilize ES to nanotube-coated surfaces, recombinant human ES/Fc chimera (R&D Systems, Minneapolis, MN, USA) at a concentration of 2.5 μg/mL was perfused through microtubes at 0.02 mL/min (Fig. 1C). ES was incubated for 2.5 h at RT in nanotube-coated microtubes, and smooth microtubes in the absence of nanotubes. In some experiments, smooth and nanotube-coated surfaces were treated with 20 μg/mL Protein-G for 2 h at RT to allow for subsequent incubation and binding of both ES (2.5 μg/mL) and anti-EpCAM (50 μg/mL; clone 158210, R&D Systems, Minneapolis, MN, USA) for 2 h at RT. All surfaces were blocked for nonspecific cell adhesion for 1 h via perfusion and incubation with 5% (w/v) bovine serum albumin (BSA, Sigma Aldrich) at 0.02 mL/min. ES was activated with calcium enriched flow buffer for 5 min prior to cell capture experiments.

ES Surface Adsorption Assay

To assess the adsorption of ES onto smooth and nanostructured surfaces, anti-human CD62E (BD Biosciences, San Jose, California, USA) conjugated to an allophycocyanin (APC) fluorophore was perfused through microtubes at 0.02 mL/min for 2.5 h following incubation with ES protein and BSA as described above. Unbound CD62E antibody was washed from microtubes using flow buffer. High resolution fluorescent images of adsorbed ES were taken at 90X magnification of each microtube using an IX-81 inverted microscope linked to a Hitachi CCD camera (Hitachi, Japan). Fluorescent images were analyzed using a three dimensional (3D) surface plot plug-in for ImageJ to obtain pixel intensity data and create 3D surface plots of ES fluorescence intensities of the microtube surfaces.

Scanning Electron Microscopy (SEM)/Atomic Force Microscopy (AFM) Surface Characterization

To characterize nanostructured HNT surfaces using SEM, 3 cm x 3 cm polyurethane (PU) sheets (Thermo Scientific, USA) were treated with poly-L-lysine solution (0.02% w/v in water) for 5 min. 100 μL of (1.1 wt %) HNT and NaL-HNT were dried on PU sheets and sputter coated with Au prior to scanning electron microscopy (SEM) analysis. SEM images of HNT and NaL-HNT immobilized onto PU surfaces were acquired using a Leica Stereoscan 440 scanning electron microscope (Leica Microsystems GmbH, Wetzlar, Germany). For atomic force microscopy (AFM) characterization, NaL-HNT and HNT-coated surfaces were prepared on polystyrene microscope slides (Thermo Fisher Scientific, Rochester, NY, USA) using an 8-well flexiPERM gasket (Sigma-Aldrich) using the same immobilization method used for SEM sample preparation. Samples were then characterized using a Veeco DI-3000 AFM (Veeco Instruments, Inc., Woodbury, NY). 10 μm x 10 μm images were recorded at random locations on each sample. Images of NaL-HNT and HNT-coated samples were analyzed in WSxM 5.0 software[41] to inspect the surface height profiles and root-mean-square (RMS) surface roughness. The following equation was used to calculate RMS values for nanostructured surfaces:

$$RMS = \left(\sum_{n=1}^{N} \left(\left(Z_n - \bar{Z} \right)^2 / N \right) \right)^{1/2}$$

where $\bar{Z}$ is the mean value of the surface height and N is the number of points in the sample[42].

Epithelial Cell Adhesion Molecule (EpCAM) Surface Expression Quantification

EpCAM surface expression on tumor cells was determined using flow cytometry. All tumor cell samples (10^5 cells) were incubated with either an APC-conjugated isotype or APC-conjugated EpCAM antibodies (1:100 dilution; Biolegend, San Diego, CA, USA) for 1 h at 4°C. Cell were then washed twice with buffer and EpCAM expression was assessed using an Accuri C6 flow cytometer (Accuri Cytometers Incorporated, Ann Arbor, MI, USA). Flow cytometry plots were generated using Accuri CFlow Plus and FlowJo Software (Treestar, Inc., San Carlos, CA, USA).

Cell Capture and Isolation Assays

Cell suspensions were perfused through microtubes using a motorized syringe pump and monitored via an inverted microscope linked to a Hitachi CCD KP-M1AN camera (Hitachi, Japan) and a Sony DVD Recorder DVO-1000MD (Sony Electronics Inc., San Diego, California, USA). Tumor cells were initially perfused at 0.008 mL/min (wall shear stress of 0.5 dyn/cm^2) for 15 min, and then 0.04 mL/min (wall shear stress of 2.5 dyn/cm^2) for 45 min. Neutrophils were perfused through microtubes at 0.04 mL/min for 60 min. The number of adhered cells was taken from 20 random video frames for each microtube. Tumor cell and neutrophil rolling adhesion at 0.04 mL/min was quantified using ImageJ software. Only cells that translated for more than 10 s, without stop-and-go motion, while remaining in the field of view (650 μm x 300 μm, 20X objective) were used to calculate the average rolling velocity. Captured cells denote cells that remained stationary on the microtube surface under flow. After flow exposure, microtube devices were washed with cell-free flow buffer, and adherent cells were removed from the tube by introducing trypsin-EDTA (0.25%) for 10 min at 37°C. Isolated cells were enumerated, and 10^4 tumor cells were plated onto glass bottom petri dishes (Grenier Bioone, Frickenhausen, Germany) and allowed to recover in media supplemented with 30% FBS for 4 h. Tumor cells were then cultured and viability assessed over a 96 h period. Viability counts were performed at 48 h and 96 h post-isolation on a hemocytometer (Hausser Scientific, Horsham, PA) using trypan blue stain. As a viability control, tumor cell samples (10^4 cells) from culture were assessed for viability 48 h and 96 h after removal from original culture using the same protocol.

Statistical Analysis

All data sets were plotted and analyzed using Microsoft Excel (Microsoft, Redmond, WA, USA) and GraphPad Prism 5.0 (GraphPad software, San Diego, CA, USA). Results from experiments were reported as the mean +/− standard error of the mean (SEM) or standard deviation (SD) as indicated. Two-tailed paired and unpaired t-tests, and one-way ANOVA with Tukey post-tests were utilized for statistical analyses. P-values less than 0.05 were considered significant.

RESULTS AND DISCUSSION

Nanotube Functionalization with Sodium Dodecanoate (NaL) Alters Dispersion Stability and Surface Charge

We initially sought to exploit the positively charged inner lumen of halloysite nanotubes (HNT) to adsorb the surfactant sodium dodecanoate (NaL), which possesses negative functional head groups needed to adsorb to the inner lumen of HNT[38]. HNT aqueous dispersibility is affected by hydrophobic interactions as well as electrostatic effects[38]. After adsorption via mixing (Figure 1A), HNT functionalized with NaL surfactant (NaL-HNT) formed stable dispersions, compared to untreated HNT which rapidly sediment (Figure 1B). Additionally, NaLHNT had an increased negative zeta potential compared to HNT (Table 1), likely due to NaL surfactant partially neutralizing the positive charge of the HNT lumen and thus increasing the overall negative charge. This increase in negative charge also enhances the ability of HNT to interact with water via charge-dipole interactions, thus increasing stability (Figure 1B). ES adsorption to NaL-HNT and HNT had minimal effects

on the overall nanotube zeta potential (Table 1). These data suggest that functionalization with NaL alters both charge and the dispersion stability of HNT.

Immobilized Surfactant-Nanotube Complexes Form Nanostructured Biomaterial Surfaces

To evaluate the ability of surfactant-nanotube complexes to form nanostructured surfaces, we characterized both NaL-HNT and HNT samples using SEM and AFM. SEM images revealed that, regardless of functionalization with surfactant, both immobilized NaL-HNT and HNT on poly-L-lysine coated polyurethane surfaces formed filamentous nanostructured surfaces, with nanotubes protruding from all surfaces (Fig 2A). AFM images further confirmed that both immobilized NaL-HNT and HNT formed surfaces with feature heights varying at the nanometer scale (Figure 2B). RMS roughness values calculated from AFM images were found to be within the range of 130~170 nm (Table 2), previously shown to enhance tumor cell adhesion via increased focal adhesion complex formation[43]. These results suggest that HNT functionalization with NaL surfactant does not alter the ability to immobilize HNT for the formation of nanostructured biomaterial surfaces.

Nanostructured Surfaces Promote Adsorption of ES

To evaluate the effects of functionalized nanostructured surfaces on the adsorption of adhesion receptors, we perfused and immobilized ES on HNT and NaL-HNT surfaces and labeled the surfaces with fluorescent ES antibodies to assess protein fluorescence intensity. High-magnification fluorescence images revealed that immobilized fluorescent ES was present on smooth surfaces (Fig. 3A) as well as on immobilized NaL-HNT (Fig. 3B) and HNT (Fig. 3C) surfaces. 3D fluorescence intensity plots were constructed from fluorescent images to reveal the fluorescence intensities of immobilized ES across the image field of view (Fig. 3D-F). Surface plots show that immobilized NaL-HNT and HNT nanostructured surfaces both increase ES surface adsorption, with both surfaces possessing significantly increased average ES fluorescence intensities compared to smooth surfaces with immobilized ES (Fig. 3G).

The increase in protein adhesion to HNT surfaces compared to smooth surfaces is likely the result of the increase in surface area produced by HNT, which has previously been shown by our lab to increase the surface area available for protein adsorption [33]. The differences between ES adsorption on NaL-HNT and HNT could be due to changes in HNT surface charge, since the differences in roughness between NaL-HNT and HNT surfaces were minimal (Table 2). With an isoelectric point at pH 5.2, ES is expected to bear a net negative charge at physiologic pH. Thus, decreased ES adsorption on NaL-HNT could be due to electrostatic repulsion between negatively charged ES and NaL-HNT of increased negative charge. These data suggest that HNT-coated surfaces enhance ES adsorption due to increased surface area, and adsorption can be further altered by changes in HNT charge.

Surfactant-Nanotube Complexes Induce a Switch From Rolling to Firm Tumor Cell Adhesion on ES Under Flow

We have developed reactive biomaterial surfaces that have previously been utilized for the study of leukocyte, stem cell, and tumor cell adhesive interactions under flow[44]-[46]. Here, the effect of immobilized surfactant-nanotube complexes on ES-mediated adhesion of tumor

cells under flow was assessed. Sialylated carbohydrate ligands are expressed on the surface of many tumor cell types, which can induce rolling tumor cell adhesion on ES [47],[48]. We initially studied COLO 205 colon cancer cell and MCF7 breast cancer cell adhesion to ES on immobilized surfactant-nanotube surfaces, given that they have been shown to interact with ES under physiologically-relevant shear stresses [47],[49],[50].

COLO 205 tumor cells adhesively interacted with smooth surfaces coated with ES under flow, with an increased number of tumor cells interacting with ES on nanostructured HNT surfaces (Figure 4A). Nanostructured surfaces consisting of surfactant-nanotube complexes further increased the number of tumor cells recruited from flow (Figure 4A). In addition to the changes in the number of tumor cells adhering to ES on smooth, HNT, and NaL-HNT coated surfaces, the strength of tumor cell adhesion was determined by measuring cell rolling velocities on ES. Rolling velocities of COLO 205 on ES significantly decreased on surfaces coated with HNT compared to smooth surfaces (Fig. 4B), which is characteristic of stronger adhesion to ES[51]. Interestingly, no rolling velocities were measured for COLO 205 tumor cells adhered to ES on NaL-HNT surfaces, as cells immediately exhibited firm adhesion and capture from flow (Fig. 4B). Breast adenocarcinoma MCF7 cells also did not exhibit rolling adhesion and were firmly adherent to ES on NaL-HNT, and no significant differences were found in MCF7 rolling velocities on ES for smooth and HNT surfaces (Fig. 4C).

Together, these data suggest that roughened surfaces comprised of surfactant-nanotube complexes can induce a switch from ES-mediated rolling to firm tumor adhesion under flow. It is interesting to note that NaL-HNT surfaces induced firm adhesion of cancer cells from flow with ES only, whereas prior studies required a capture antibody to ensure rare cell separation from flow, including CTCs and stem cells. Rare hematopoietic stem and progenitor cell (HSPC) isolation procedures typically necessitate the use for antibodies against stem cell marker CD34[52]. CTCs have previously been captured using antibodies against epithelial cell adhesion molecule (EpCAM)[24] or prostate-specific membrane antigen (PSMA) for prostate-based CTCs[15]. However, these techniques are not comprehensive, given the phenotype heterogeneity of CTCs. For the diagnosis and treatment of metastatic cancer, the current technique provides a more comprehensive approach to isolate CTCs, regardless of biomarker expression, and in the absence of capture antibodies. For example, this technique could be used to isolate CTCs that are EpCAM(−), which have been shown to be competent for brain metastasis in the case of breast cancer CTCs[32], in addition to EpCAM+ cells.

Surfactant-Nanotube Complexes Reduce Leukocyte Adhesion to ES Under Flow

Previous studies have shown that leukocytes exhibit rolling adhesion on ES in parallel plate flow chambers *in vitro* [9],[53],, and adhere to ES expressed on the endothelium *in vivo*[54],[55]. Thus, improvement of CTC purity levels using flow-based devices consisting of immobilized ES is challenged by the fact that both CTCs and leukocytes possess ligands for ES. Additionally, 1 CTC is present for approximately every one million leukocytes in a given patient blood sample, posing a “needle in a haystack” problem for CTC isolation [25]. Here, we sought to assess the adhesion of leukocytes to ES on surfactant-nanotube

complexes under flow. It was observed that more human neutrophils adhesively interact with ES on smooth surfaces compared to HNT-coated surfaces (Fig. 5A). Surfactant-nanotube complexes further decreased the number of neutrophils adhesively interacting with ES under flow (Fig. 5A). Analysis of neutrophil rolling velocities on ES revealed no significant differences on smooth, HNT, and NaL-HNT coated surfaces (Fig. 5B). However, the average number of neutrophils firmly adhered to ES significantly decreased on NaL-HNT compared to untreated HNT (Fig. 5C). These data suggest that nanostructured surfaces consisting of surfactant-nanotube complexes reduce leukocyte adhesion to ES. The reduction in leukocyte adhesion to ES on surfactant-nanotube complexes is likely due to a combination of surface roughness and surface charge. Our lab has previously observed reduced numbers of adherent leukocytes and reduced leukocyte spreading on nanostructured surfaces compared to smooth surfaces, indicative of weakened adhesion [(15),(21)]. Our current work shows that HNT functionalization with NaL surfactant acts to increase the overall negative HNT charge (Table 1). Given that neutrophils possess a negatively charged surface [(56)], it is possible that the increased negative charge of HNT acts to repel neutrophils from coming within a reactive distance to ES on surfactant-nanotube complexes. Future work should examine neutrophil adhesion to nanostructured surfaces over a range of surface charges to determine the relationship between adhesion and surface charge.

Surfactant-Nanotube Complexes Induce Selectin-Mediated Capture of Tumor Cells in the Absence of Capture Antibodies

To assess the ability of surfactant-nanotube complexes to induce selectin-mediated capture of tumor cells in the absence of antibodies, we compared the effects of immobilized NaL-HNT complexes on ES-mediated capture of tumor cells to capture methods that require a capture antibody, such as anti-EpCAM antibodies. Lung carcinoma A549 and breast carcinoma Hs 578T cell lines were chosen as model CTCs, given their ability to adhesively interact with ES[(57)-(60)]. Additionally, A549 and Hs 578T were chosen for capture assays because they express low and negligible EpCAM on their surface, respectively [(61),(62)]. Both tumor cell types thus are not efficiently isolated using methods that require capture antibodies such as anti-EpCAM.

Compared to COLO 205 and MCF7 tumor cell lines, which highly expressed EpCAM on their surface (Figure 6A,B), flow cytometry analysis showed low to negligible EpCAM surface expression on A549 and Hs 578T tumor cells, respectively (Figure 6C,D). In tumor cell capture assays, while some A549 tumor cells adhesively interacted with smooth biomaterial surfaces coated with ES and anti-EpCAM, it was observed that tumor cell adhesion increased on NaLHNT nanostructured biomaterials coated with ES only (Figure 7A). A549 tumor cell capture was significantly increased on NaL-HNT biomaterials coated with ES, compared to smooth and HNT surfaces coated with both ES and anti-EpCAM (Figure 7B). The addition of anti-EpCAM on NaL-HNT surfaces had no significant effect on tumor cell capture, demonstrating that tumor cells can be efficiently captured on NaL-HNT surfaces coated with ES in the absence of capture antibodies (Figure 7B). These differences in adhesion and capture were even more apparent with Hs 578T tumor cells, which express negligible EpCAM on their surface [(61),(62)]. Given negligible EpCAM expression, very low numbers of Hs 578T tumor cells adhered to smooth surfaces coated

with ES and anti-EpCAM (Figure 7C). A large increase in Hs 578T tumor cell adhesion was observed on NaL-HNT surfaces coated with ES only (Figure 7C). A negligible number of Hs 578T tumor cells were captured on smooth surfaces coated with ES and anti-EpCAM (Figure 7D). While a small number of tumor cells were captured on HNT surfaces coated with ES and anti-EpCAM, tumor cell capture significantly increased on NaL-HNT surfaces coated only with ES (Figure 7D). As with A549 cells, the addition of anti-EpCAM had no significant effect on tumor cell capture on NaL-HNT surfaces (Figure 7D). Captured A549 and Hs578T tumor cells isolated from surfaces remained viable in culture, as no significant differences in viability were observed over a 96 h culture span compared to tumor cells isolated from culture (Figure 8).

While the exact mechanism behind enhanced tumor cell adhesion to surfactant-nanotube complexes remains to be determined, this adhesion phenomenon could be due to tumor cell glycocalyx, a gel-like layer of biologically inert macromolecules on the CTC surface that can extend as far as 500 nm from the CTC surface[63]. In particular, the synthesis of glycocalyx components can be impaired during malignant transformation, causing cancer cells to greatly overexpress the glycocalyx component hyaluronan on their surface[64],[65]. It is possible that NaL could act as an adhesion ligand to the tumor cell glycocalyx, and future studies evaluating the effect of glycocalyx coatings could shed further light on the mechanisms contributing to increased tumor cell adhesion to surfactant-nanotube complexes.

CONCLUSION

The present study demonstrates that immobilized surfactant-nanotube complexes enhance tumor cell adhesion to ES, and can be exploited to capture tumor cells in the absence of capture antibodies typically required for CTC isolation. HNT were functionalized with the surfactant NaL, which increased HNT negative charge and dispersion stability. HNT were functionalized with the surfactant NaL without altering their immobilization on biomaterials to form nanostructured surfaces. Adsorption of ES was enhanced on surfactant-nanotube coated surfaces compared to smooth surfaces alone. In adhesion assays, tumor cells that typically exhibit rolling adhesion on ES-coated smooth surfaces were firmly adhered and captured from flow on surfactant-nanotube complexes. Compared to flow-based assays consisting of immobilized ES and anti-EpCAM, ES-coated NaL-HNT captured significantly more tumor cells from flow. This unique adhesion phenomenon was exploited to capture highly metastatic tumor cells that have low to negligible EpCAM surface expression, which typically elude conventional CTC isolation assays that utilize antibody-based capture. In contrast to the FDA-approved CellSearch® CTC isolation method, this flow-based isolation did not significantly affect tumor cell viability. This rapid, simple method to create surfactant-nanotube complexes provides a unique platform to isolate CTCs that are heterogeneous in phenotype, for the development of personalized medicine regimens for patients with highly metastatic hematogenous cancers such as those originating in lung, breast, and prostate.

ACKNOWLEDGEMENTS

The authors gratefully acknowledge Jeff Mattison for work with blood sample collection and donor recruitment. The work described was supported by the Cornell Center on the Microenvironment and Metastasis through Award Number U54CA143876 from the National Cancer Institute. The content is solely the responsibility of the authors and does not necessarily represent the official views of the National Cancer Institute or the National Institutes of Health. This work made use of the Cornell Center for Materials Research Shared Facilities which are supported through the NSF MRSEC program (DMR-1120296).

REFERENCES

1. Chaffer CL, Weinberg RA. A Perspective on Cancer Cell Metastasis. Science. 2011; 331:1559–64. [PubMed: 21436443]
2. Chang YS, di Tomaso E, McDonald DM, Jones R, Jain RK, Munn LL. Mosaic blood vessels in tumors: frequency of cancer cells in contact with flowing blood. Proc Natl Acad Sci USA. 2000; 97:14608–13. [PubMed: 11121063]
3. Butler TP, Gullino PM. Quantitation of cell shedding into efferent blood of mammary adenocarcinoma. Cancer Research. 1975; 35:512–6. [PubMed: 1090362]
4. Riethdorf S, Wikman H, Pantel K. Review: Biological relevance of disseminated tumor cells in cancer patients. International Journal of Cancer. 2008; 123:1991–2006.
5. Maheswaran S, Haber DA. Circulating tumor cells: a window into cancer biology and metastasis. Current Opinion in Genetics & Development. 2010; 20:96–9. [PubMed: 20071161]
6. Mitchell MJ, King MR. Computational and experimental models of cancer cell response to fluid shear stress. Frontiers in Oncology. 2013; 3:1–11. [PubMed: 23373009]
7. Mitchell MJ, King MR. Fluid shear stress sensitizes cancer cells to receptor-mediated apoptosis via trimeric death receptors. New Journal of Physics. 2013; 15:015008. [PubMed: 25110459]
8. Coussens LM, Werb Z. Inflammation and cancer. Nature. 2002; 420:860–7. [PubMed: 12490959]
9. Lawrence MB, Springer TA. Neutrophils roll on E-selectin. The Journal of Immunology. 1993; 151:6339–46.
10. McDonald B, Spicer J, Giannais B, Fallavollita L, Brodt P, Ferri L. Systemic inflammation increases cancer cell adhesion to hepatic sinusoids by neutrophil mediated mechanisms. International Journal of Cancer. 2009; 125:1298–305.
11. van Ginhoven TM, van den Berg JW, Dik WA, Ijzermans JNM, de Bruin RWF. Preoperative dietary restriction reduces hepatic tumor load by reduced E-selectin- mediated adhesion in mice. J Surg Oncol. 2010; 102:348–53. [PubMed: 20672315]
12. Gassmann P, Kang ML, Mees ST, Haier J. In vivo tumor cell adhesion in the pulmonary microvasculature is exclusively mediated by tumor cell--endothelial cell interaction. BMC Cancer. 2010; 10:177. [PubMed: 20433713]
13. Yin X, Rana K, Ponmudi V, King MR. Knockdown of fucosyltransferase III disrupts the adhesion of circulating cancer cells to E-selectin without affecting hematopoietic cell adhesion. Carbohydrate Research. 2010; 345:2334–42. [PubMed: 20833389]
14. Rahn JJ, Chow JW, Horne GJ, Mah BK, Emerman JT, Hoffman P, Hugh JC. MUC1 mediates transendothelial migration in vitro by ligating endothelial cell ICAM-1. Clinical & Experimental Metastasis. 2005; 22:475–83. [PubMed: 16320110]
15. Hughes AD, Mattison J, Western LT, Powderly JD, Greene BT, King MR. Microtube Device for Selectin-Mediated Capture of Viable Circulating Tumor Cells from Blood. Clinical Chemistry. 2012; 58:846–53. [PubMed: 22344286]
16. Hughes AD, Mattison J, Powderly JD, Greene BT, King MR. Rapid Isolation of Viable Circulating Tumor Cells from Patient Blood Samples. JoVE. MyJoVE Corporation. 2012:e4248–8.
17. Luo X, Mitra D, Sullivan RJ, Wittner BS, Kimura AM, Pan S, Hoang MP, Brannigan BW, Lawrence DP, Flaherty KT, Sequist LV, McMahon M, Bosenberg MW, Stott SL, Ting DT, Ramaswamy S, Toner M, Fisher DE, Maheswaran S, Haber DA. Isolation and Molecular Characterization of Circulating Melanoma Cells. Cell Rep. 2014

18. Mitchell, MJ.; King, MR. Expert Rev Anticancer Ther. Vol. 14. Informa UK, Ltd; 2014. Unnatural killer cells to preventbloodborne metastasis: inspiration frombiology and engineering.; p. 641-4.
19. Mitchell MJ, Wayne E, Rana K, Schaffer CB, King MR. TRAIL-coated leukocytes that kill cancer cells in the circulation. Proc Natl Acad Sci USA. 2014; 111:930–5. [PubMed: 24395803]
20. Mitchell MJ, Chen CS, Ponmudi V, Hughes AD, King MR. E-selectin liposomal and nanotube-targeted delivery of doxorubicin to circulating tumor cells. Journal of Controlled Release. 2012; 160:609–17. [PubMed: 22421423]
21. Mitchell MJ, Castellanos CA, King MR. Nanostructured Surfaces to Target and Kill Circulating Tumor Cells While Repelling Leukocytes. Journal of Nanomaterials. 2012; 2012:1–10.
22. Mitchell MJ, King MR. Leukocytes as carriers for targeted cancer drug delivery. Expert Opin Drug Deliv. 2014:1–18.
23. Greene BT, Hughes AD, King MR. Circulating Tumor Cells: The Substrate of Personalized Medicine? Frontiers in Oncology. 2012; 2:1–6.
24. Allard WJ, Matera J, Miller MC, Repollet M, Connelly MC, Rao C, Tibbe AGJ, Uhr JW. Terstappen LWMM. Tumor cells circulate in the peripheral blood of all major carcinomas but not in healthy subjects or patients with nonmalignant diseases. Clin Cancer Res. 2004; 10:6897–904. [PubMed: 15501967]
25. Hughes AD, King MR. Nanobiotechnology for the capture and manipulation of circulating tumor cells. WIREs Nanomed Nanobiotechnol [Internet]. 2011; 4:291–309. Available from: http://onlinelibrary.wiley.com/doi/10.1002/wnan.168/full.
26. Yu M, Stott S, Toner M, Maheswaran S, Haber DA. Circulating tumor cells: approaches to isolation and characterization. The Journal of Cell Biology. 2011; 192:373–82. [PubMed: 21300848]
27. Miller MC, Doyle GV, Terstappen LWMM. Significance of Circulating Tumor Cells Detected by the CellSearch System in Patients with Metastatic Breast Colorectal and Prostate Cancer. J Oncol. 2010; 2010:617421. [PubMed: 20016752]
28. Nagrath S, Sequist LV, Maheswaran S, Bell DW, Irimia D, Ulkus L, Smith MR, Kwak EL, Digumarthy S, Muzikansky A, Ryan P, Balis UJ, Tompkins RG, Haber DA, Toner M. Isolation of rare circulating tumour cells in cancer patients by microchip technology. Nature. 2007; 450:1235–9. [PubMed: 18097410]
29. Bajpai S, Mitchell MJ, King MR, Reinhart-King CA. A microfluidic device to select for cells based on chemotactic phenotype. Technology. 2014; 02:101–5. [PubMed: 24999488]
30. Hughes AD, Marshall JR, Keller E, Powderly JD, Greene BT, King MR. Differential drug responses of circulating tumor cells within patient blood. Cancer Letters. 2013
31. Yu M, Bardia A, Wittner BS, Stott SL, Smas ME, Ting DT, Isakoff SJ, Ciciliano JC, Wells MN, Shah AM, Concannon KF, Donaldson MC, Sequist LV, Brachtel E, Sgroi D, Baselga J, Ramaswamy S, Toner M, Haber DA, Maheswaran S. Circulating Breast Tumor Cells Exhibit Dynamic Changes in Epithelial and Mesenchymal Composition. Science. 2013; 339:580–4. [PubMed: 23372014]
32. Zhang L, Ridgway LD, Wetzel MD, Ngo J, Yin W, Kumar D, Goodman JC, Groves MD, Marchetti D. The identification and characterization of breast cancer CTCs competent for brain metastasis. Science Translational Medicine. 2013; 5:180ra48.
33. Hughes AD, King MR. Use of Naturally Occurring Halloysite Nanotubes for Enhanced Capture of Flowing Cells. Langmuir. American Chemical Society. 2010; 26:12155–64.
34. Liu, M.; Guo, B.; Du, M.; Cai, X.; Jia, D. Nanotechnology. Vol. 18. IOP Publishing; 2007. Properties of halloysite nanotube-epoxy resin hybrids and the interfacial reactions in the systems.; p. 455703
35. Abdullayev E, Joshi A, Wei W, Zhao Y, Lvov Y. Enlargement of halloysite clay nanotube lumen by selective etching of aluminum oxide. ACS Nano. 2012; 6:7216–26. [PubMed: 22838310]
36. Lvov YM, Shchukin DG, Möhwald H, Price RR. Halloysite clay nanotubes for controlled release of protective agents. ACS Nano. 2008; 2:814–20. [PubMed: 19206476]
37. Veerabadran NG, Price RR, Lvov YM. Clay Nanotubes for Encapsulation and Sustained Release of Drugs. NANO. 2007; 02:115–20.

38. Cavallaro G, Lazzara G, Milioto S. Exploiting the Colloidal Stability and Solubilization Ability of Clay Nanotubes/Ionic Surfactant Hybrid Nanomaterials. J Phys Chem C. 2012; 116:21932–8.
39. Mitchell MJ, Lin KS, King MR. Fluid Shear Stress Increases Neutrophil Activation via Platelet-Activating Factor. Biophysical Journal. 2014; 106:2243–53. [PubMed: 24853753]
40. Mitchell MJ, King MR. Shear-Induced Resistance to Neutrophil Activation via the Formyl Peptide Receptor. Biophysical Journal. Biophysical Society. 2012; 102:1804–14.
41. Horcas I, Fernández R, Gómez-Rodríguez JM, Colchero J, Gómez-Herrero J, Baro AM. WSXM: a software for scanning probe microscopy and a tool for nanotechnology. Rev Sci Instrum. 2007; 78:013705. [PubMed: 17503926]
42. Khulbe, KC.; Feng, CY.; Matsuura, T. Synthetic Polymeric Membranes: Characterization by Atomic Force Microscopy. Springer; 2008. p. 1
43. Chen W, Weng S, Zhang F, Allen S, Li X, Bao L, Lam RHW, Macoska JA, Merajver SD, Fu J. Nanoroughened Surfaces for Efficient Capture of Circulating Tumor Cells without Using Capture Antibodies. ACS Nano. 2013; 7:566–75. [PubMed: 23194329]
44. Ball C, King M. Role of c-Abl in L-selectin shedding from the neutrophil surface. Blood Cells, Molecules, and Diseases. 2011; 46:246–51.
45. Rana K, Liesveld JL, King MR. Delivery of apoptotic signal to rolling cancer cells: A novel biomimetic technique using immobilized TRAIL and E-selectin. Biotechnol Bioeng. 2009; 102:1692–702. [PubMed: 19073014]
46. Cao TM, Mitchell MJ, Liesveld J, King MR. Stem Cell Enrichment with Selectin Receptors: Mimicking the pH Environment of Trauma. Sensors. 2013; 13:12516–26. [PubMed: 24048341]
47. Myung JH, Gajjar KA, Pearson RM, Launiere CA, Eddington DT, Hong S. Direct measurements on CD24-mediated rolling of human breast cancer MCF-7 cells on Eselectin. Analytical Chemistry. 2011; 83:1078–83. [PubMed: 21207944]
48. Myung JH, Gajjar KA, Saric J, Eddington DT, Hong S. Dendrimer-Mediated Multivalent Binding for the Enhanced Capture of Tumor Cells. Angew Chem. 2011; 123:11973–6.
49. Kim MB, Sarelius IH. Distributions of Wall Shear Stress in Venular Convergences of Mouse Cremaster Muscle. Microcirculation. 2003; 10:167–78. [PubMed: 12700585]
50. Rana K, Reinhart-King CA, King MR. Inducing Apoptosis in Rolling Cancer Cells: A Combined Therapy with Aspirin and Immobilized TRAIL and E-Selectin. Molecular Pharmaceutics. 2012; 9:2219–27. [PubMed: 22724630]
51. Finger E, Puri K, Alón R, Lawrence M, Andrian von U, Springer T. Adhesion through Lselectin requires a threshold hydrodynamic shear. Nature. 1996; 379:266–8. [PubMed: 8538793]
52. Narasipura SD, Wojciechowski JC, Charles N, Liesveld JL, King MR. P-Selectin coated microtube for enrichment of CD34+ hematopoietic stem and progenitor cells from human bone marrow. Clinical Chemistry. 2008; 54:77–85. [PubMed: 18024531]
53. Abbassi O, Kishimoto TK, McIntire LV, Anderson DC, Smith CW. E-selectin supports neutrophil rolling in vitro under conditions of flow. Journal of Clinical Investigation. 1993; 92:2719–30. [PubMed: 7504692]
54. Bullard DC, Kunkel EJ, Kubo H, Hicks MJ, Lorenzo I, Doyle NA, Doerschuk CM, Ley K, Beaudet AL. Infectious susceptibility and severe deficiency of leukocyte rolling and recruitment in E-selectin and P-selectin double mutant mice. The Journal of Experimental Medicine. 1996; 183:2329–36. [PubMed: 8642341]
55. O'Brien KD, McDonald TO, Chait A, Allen MD, Alpers CE. Neovascular expression of E-selectin, intercellular adhesion molecule-1, and vascular cell adhesion molecule-1 in human atherosclerosis and their relation to intimal leukocyte content. Circulation. 1996; 93:672–82. [PubMed: 8640995]
56. Parodi, A.; Quattrocchi, N.; van de Ven, AL.; Chiappini, C.; Evangelopoulos, M.; Martinez, JO.; Brown, BS.; Khaled, SZ.; Yazdi, IK.; Enzo, MV.; Isenhart, L.; Ferrari, M.; Tasciotti, E. Nature Nanotechnology. Vol. 8. Nature Publishing Group; 2012. Synthetic nanoparticles functionalized with biomimetic leukocyte membranes possess cell-like functions.; p. 61-8.
57. Fuster MM, Brown JR, Wang L, Esko JD. A disaccharide precursor of sialyl Lewis X inhibits metastatic potential of tumor cells. Cancer Research. 2003; 63:2775–81. [PubMed: 12782582]

58. Burdick, MM.; Henson, K.; Delgadillo, LF.; Choi, YE.; Goetz, DJ.; Tees, DF.; Benencia, F. Frontiers in Oncology. Vol. 2. Frontiers Media; SA: 2012. Expression of E-selectin ligands on circulating tumor cells: cross-regulation with cancer stem cell regulatory pathways?; p. 103

59. Gong L, Mi H-J, Zhu H, Zhou X, Yang H. P-selectin-mediated platelet activation promotes adhesion of non-small cell lung carcinoma cells on vascular endothelial cells under flow. Mol Med Rep. 2012; 5:935–42. [PubMed: 22266541]

60. Brown JR, Fuster MM, Whisenant T, Esko JD. Expression patterns of alpha 2,3- sialyltransferases and alpha 1,3-fucosyltransferases determine the mode of sialyl Lewis X inhibition by disaccharide decoys. J Biol Chem. 2003; 278:23352–9. [PubMed: 12686549]

61. Yoon HJ, Kim TH, Zhang Z, Azizi E, Pham TM, Paoletti C, Lin J, Ramnath N, Wicha MS, Hayes DF, Simeone DM, Nagrath S. Sensitive capture of circulating tumour cells by functionalized graphene oxide nanosheets. Nature Nanotechnology. 2013; 8:735–41.

62. Kim Y, Kim HS, Cui ZY, Lee H-S, Ahn JS, Park CK, Park K, Ahn M-J. Clinicopathological implications of EpCAM expression in adenocarcinoma of the lung. Anticancer Research. 2009; 29:1817–22. [PubMed: 19443410]

63. Mitchell MJ, King MR. Theme: Physical Biology in Cancer. 3. The role of cell glycocalyx in vascular transport of circulating tumor cells. AJP: Cell Physiology. 2014; 306:C89–C97. [PubMed: 24133067]

64. Hopwood JJ, Dorfman A. Glycosaminoglycan synthesis by cultured human skin fibroblasts after transformation with simian virus 40. Journal of Biological Chemistry. 1977; 252:4777–85. [PubMed: 194893]

65. Itano N, Kimata K. Altered hyaluronan biosynthesis in cancer progression. Seminars in Cancer Biology. 2008; 18:268–74. [PubMed: 18450474]

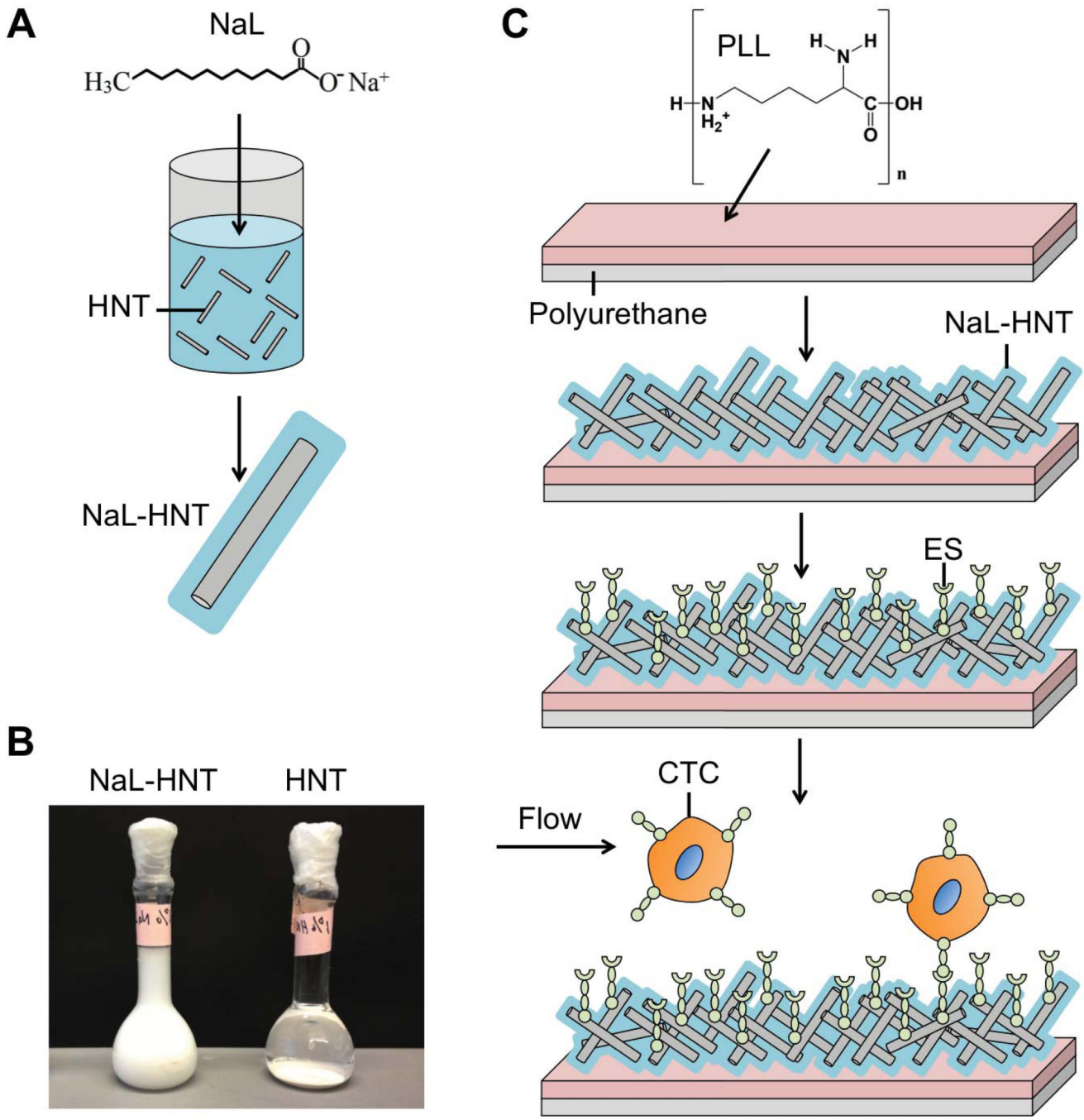

Figure 1.

Development of surfactant-nanotube complexes to fabricate nanostructured biomaterial surfaces for flow-based tumor cell capture assays. (A) Mixing and adsorption of sodium dodecanoate (NaL) surfactant to halloysite nanotubes (HNT) to create surfactant-nanotube complexes (NaL-HNT). (B) Stability of NaL-HNT and HNT dispersions (1.1 wt %) 24 h post-mixing and adsorption. (C) Fabrication of nanostructured biomaterial surfaces. Polyurethane (PU) flow device surfaces coated with poly-L-lysine (PLL) to immobilize NaL-HNT and HNT. E-selectin (ES) is then adsorbed to HNT-coated surfaces, and tumor

cells are perfused over surfaces at physiologically relevant flow rates to enable tumor cell capture. CTC: circulating tumor cell.

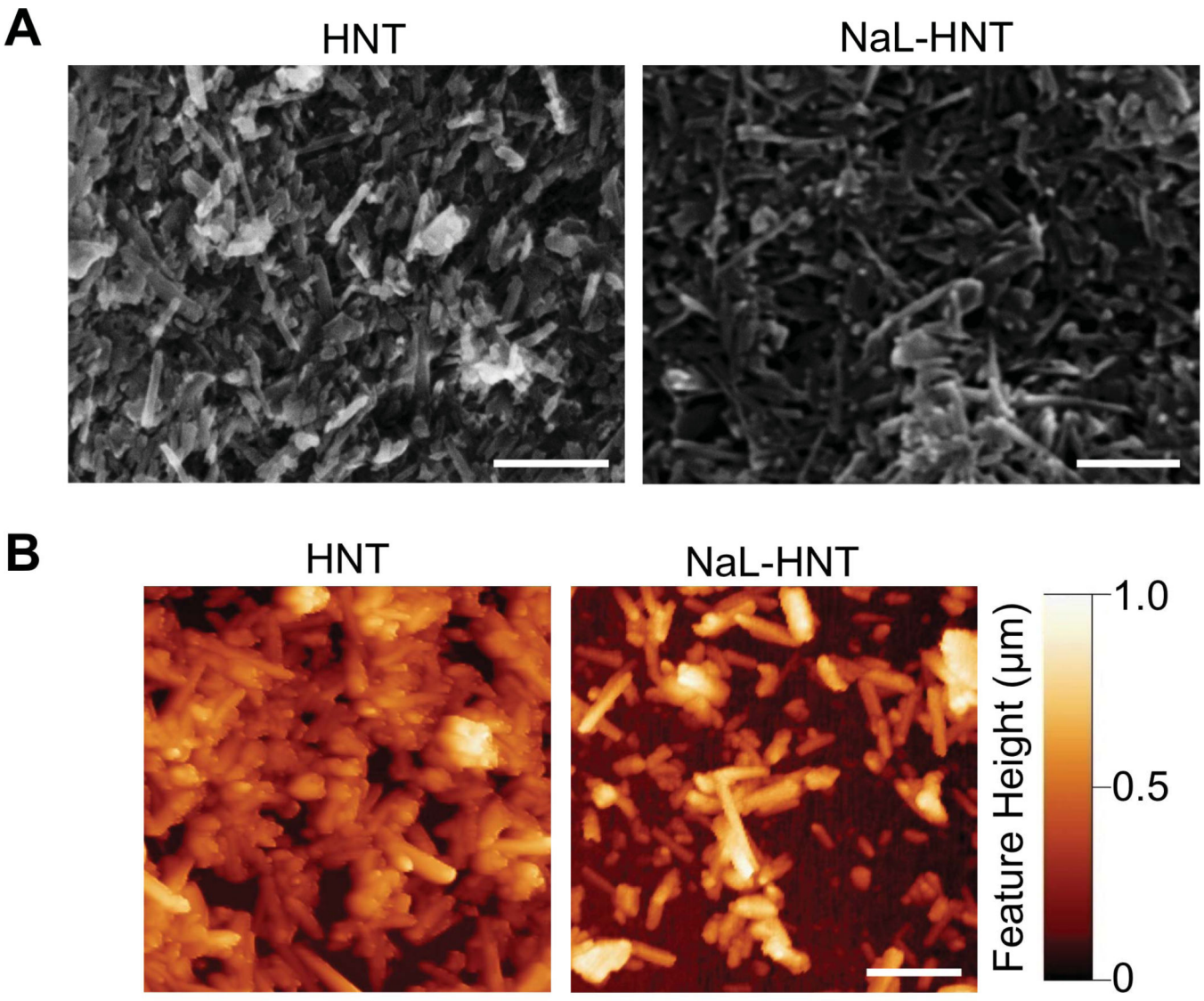

Figure 2.

Surface characterization of nanostructured biomaterial surfaces. (A) Representative SEM images of PLL-coated PU substrates with immobilized HNT and NaL-HNT. Scale bar = 2 μm. (B) Representative AFM images of PLL coated PU substrates with immobilized HNT and NaL-HNT. Scale bar = 2 μm.

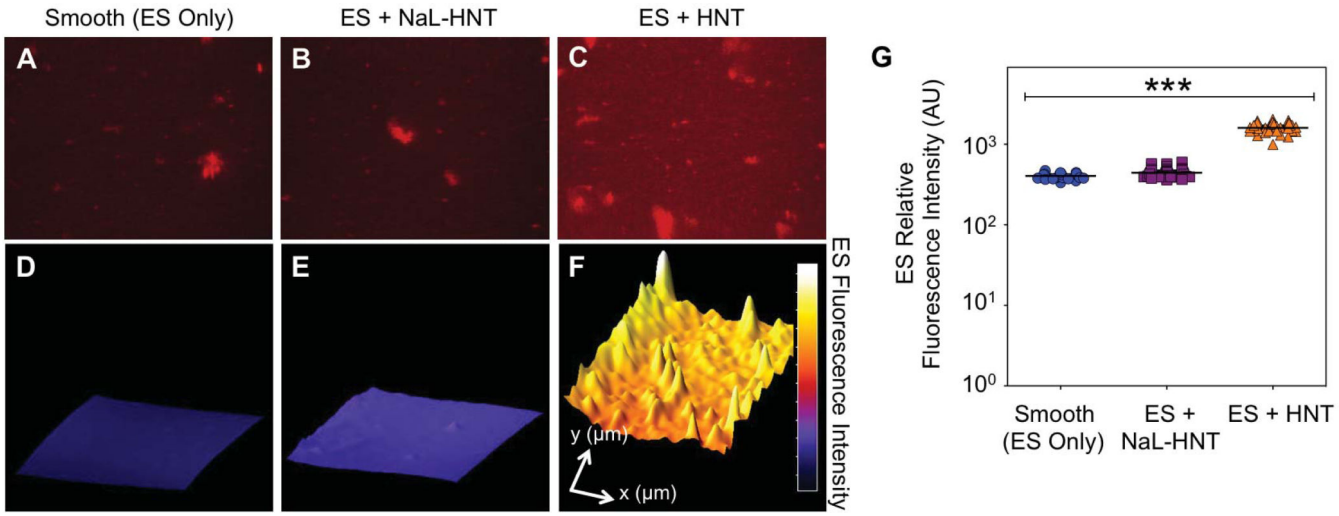

Figure 3.

Detection of immobilized ES on biomaterial surfaces. (A-C) Representative high magnification fluorescence micrographs of recombinant human ES (red) adsorbed on smooth (ES only; A) surfaces, immobilized NaL-HNT (B), and HNT (C) coated microscale flow devices. Scale bar = 40 μm. (D-F) Representative three-dimensional surface plots of immobilized recombinant human ES fluorescence intensity on smooth (D), NaL-HNT (E), and HNT (F) coated microscale flow devices. Profile length in *x*- and *y*-directions are 240 μm and 160 μm, respectively. (G) Immobilized ES relative fluorescence intensity values on smooth and nanostructured surfaces. Calculated values are mean +/- standard deviation (n = 3). Statistics were calculated using a one-way ANOVA with Tukey post test. ***P < 0.0001.

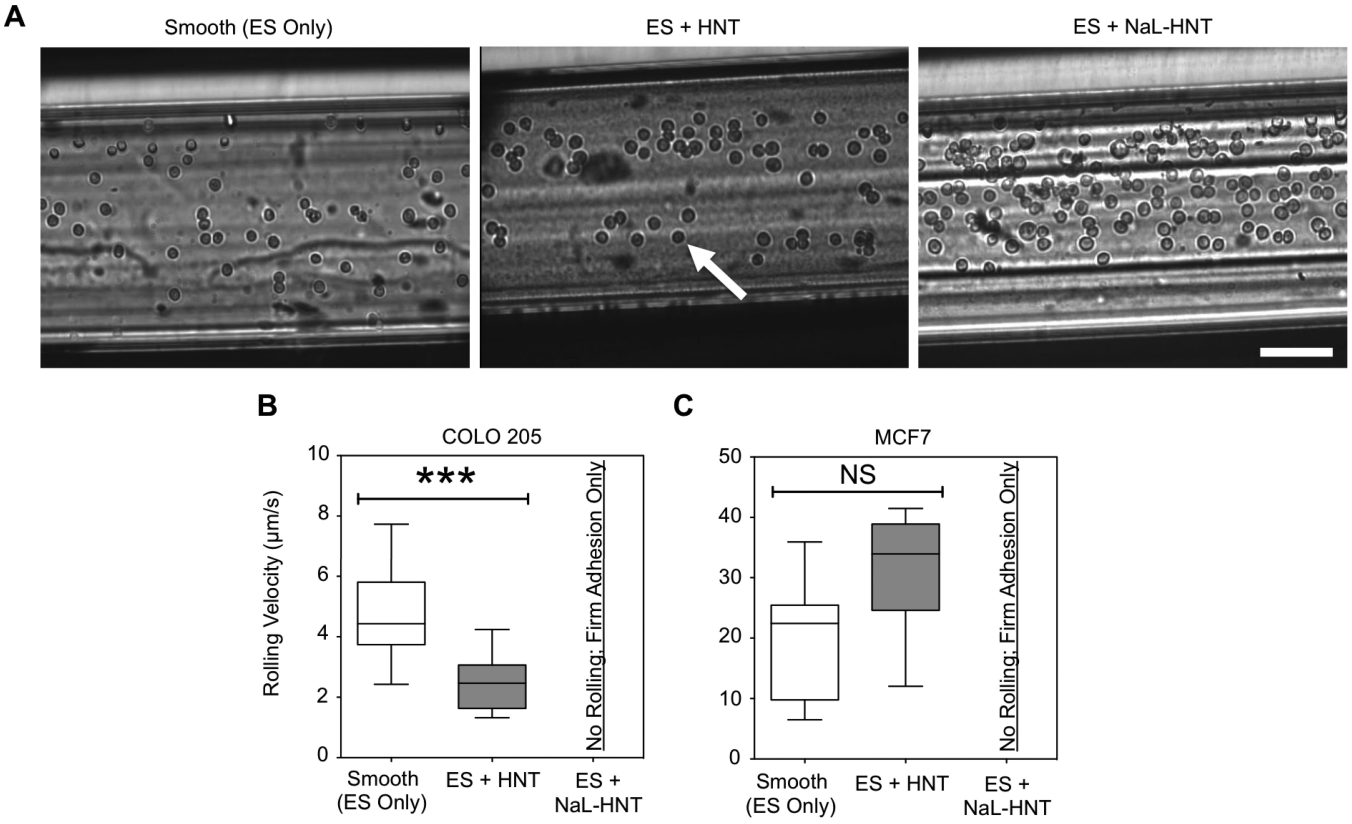

Figure 4.

ES-mediated adhesion of tumor cells to immobilized surfactant-nanotube complexes under flow. (A) Representative images of ES-mediated adhesion of COLO 205 cells under flow on smooth surfaces, immobilized HNT, and NaL-HNT coated microscale flow device biomaterial surfaces. Arrows denote adhered COLO 205 cells, which exhibit either rolling or firm adhesion. Scale bar = 100 μm. (B,C) COLO 205 (B) and MCF7 (C) tumor cell rolling velocities on ES on smooth, HNT, and NaL-HNT coated microscale flow device surfaces. Error bars denote minimum and maximum data points. Statistics were calculated using a two-tailed unpaired t-test. *NS*: not significant. ***$P < 0.0001$. n = 30 or more rolling cells analyzed for each condition.

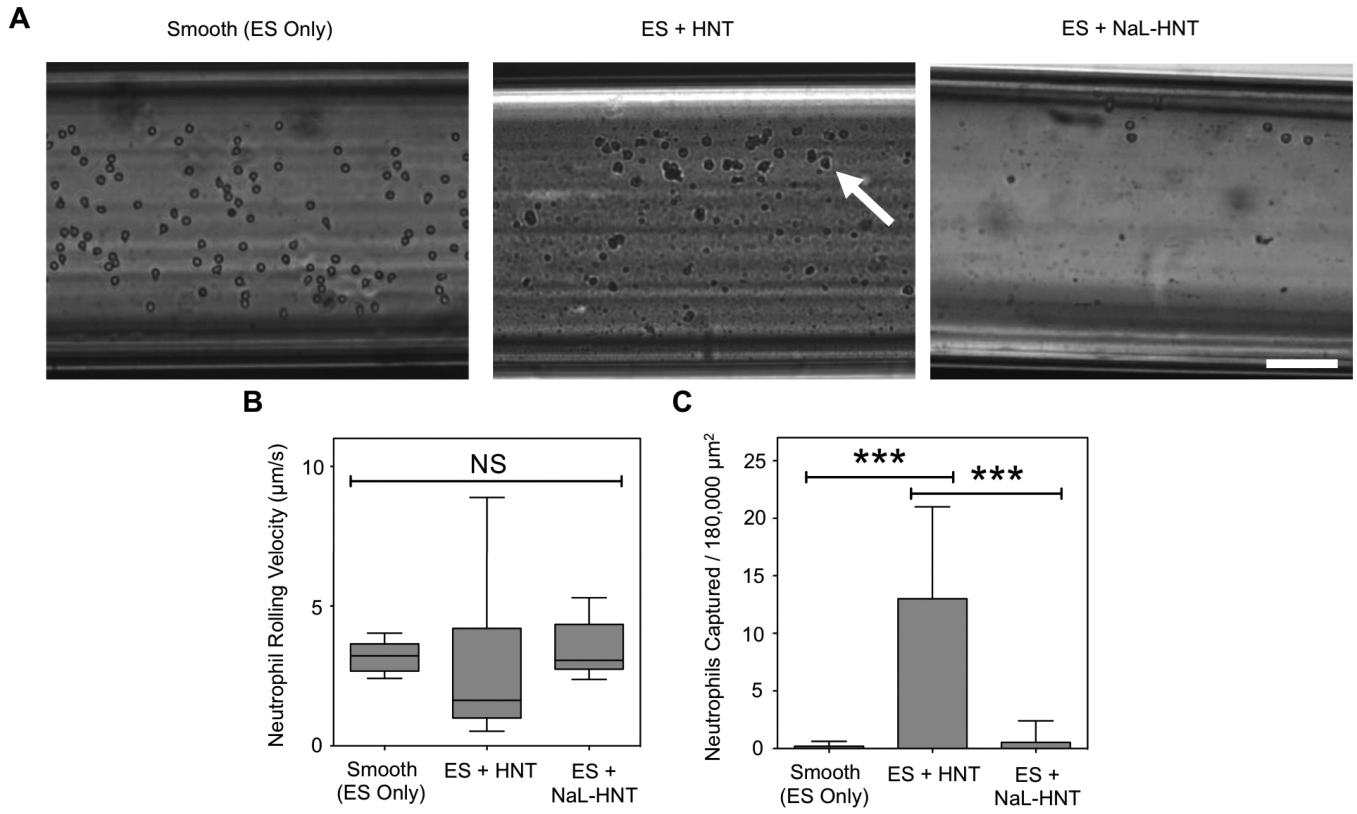

Figure 5.

ES-mediated adhesion of leukocytes to immobilized surfactant-nanotube complexes under flow. (A) Representative images of ES-mediated adhesion of primary human neutrophils under flow on smooth surfaces, immobilized HNT, and NaL-HNT coated microscale flow device biomaterial surfaces. Arrows denote adhered neutrophils, which exhibit either rolling or firm adhesion. Scale bar = 100 μm. (B) Neutrophil rolling velocities on ES on smooth, HNT, and NaL-HNT coated microscale flow device surfaces. Error bars denote minimum and maximum data points. Statistics were calculated using a two-tailed unpaired t-test. *NS*: not significant. n = 30 or more rolling cells analyzed for each condition. (C) Number of captured neutrophils per 180,000 μm^2 of biomaterial surface area. Captured neutrophils denote cells that are firmly adhered to the surface. Calculated values are mean +/- standard deviation. n = 20 or more frames analyzed for captured cells for each condition. Statistics were calculated using a one-way ANOVA with Tukey post test. ***$P < 0.0001$.

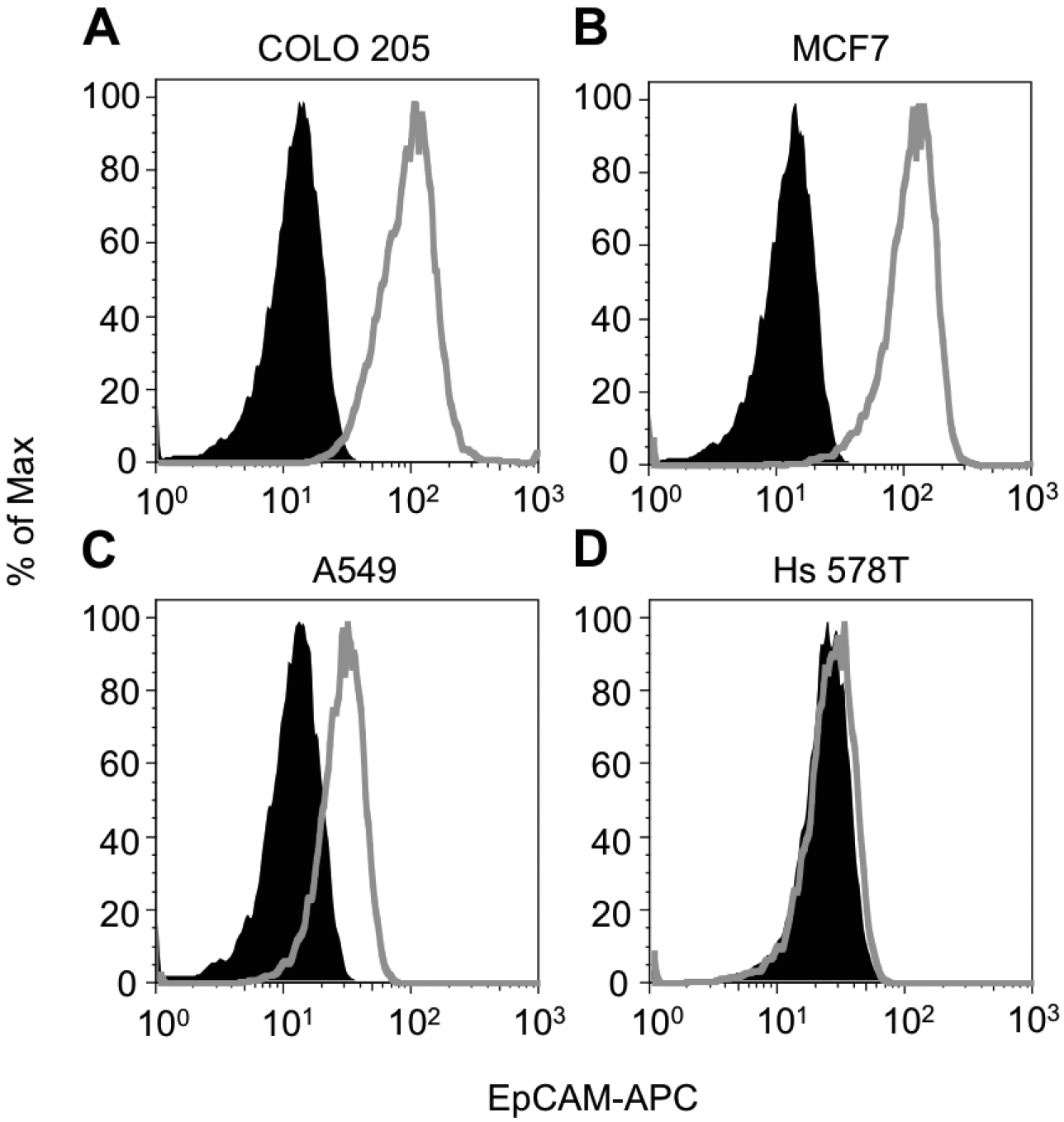

Figure 6.

Epithelial cell adhesion molecule (EpCAM) surface expression on tumor cell lines. (A-D) Flow cytometry histograms of EpCAM surface expression on COLO 205 (A), MCF7 (B), A549 (C), and Hs 578T (D) tumor cells. Grey histograms denote tumor cell samples labeled with allophycocyanin (APC) fluorescent anti-EpCAM antibodies. Black histograms denote tumor cell samples labeled with APC isotype controls. A minimum of 10^4 cells was analyzed for each sample. % Of Max: number of detected cells in each bin divided by the number of cells in the bin that contains the largest number of cells.

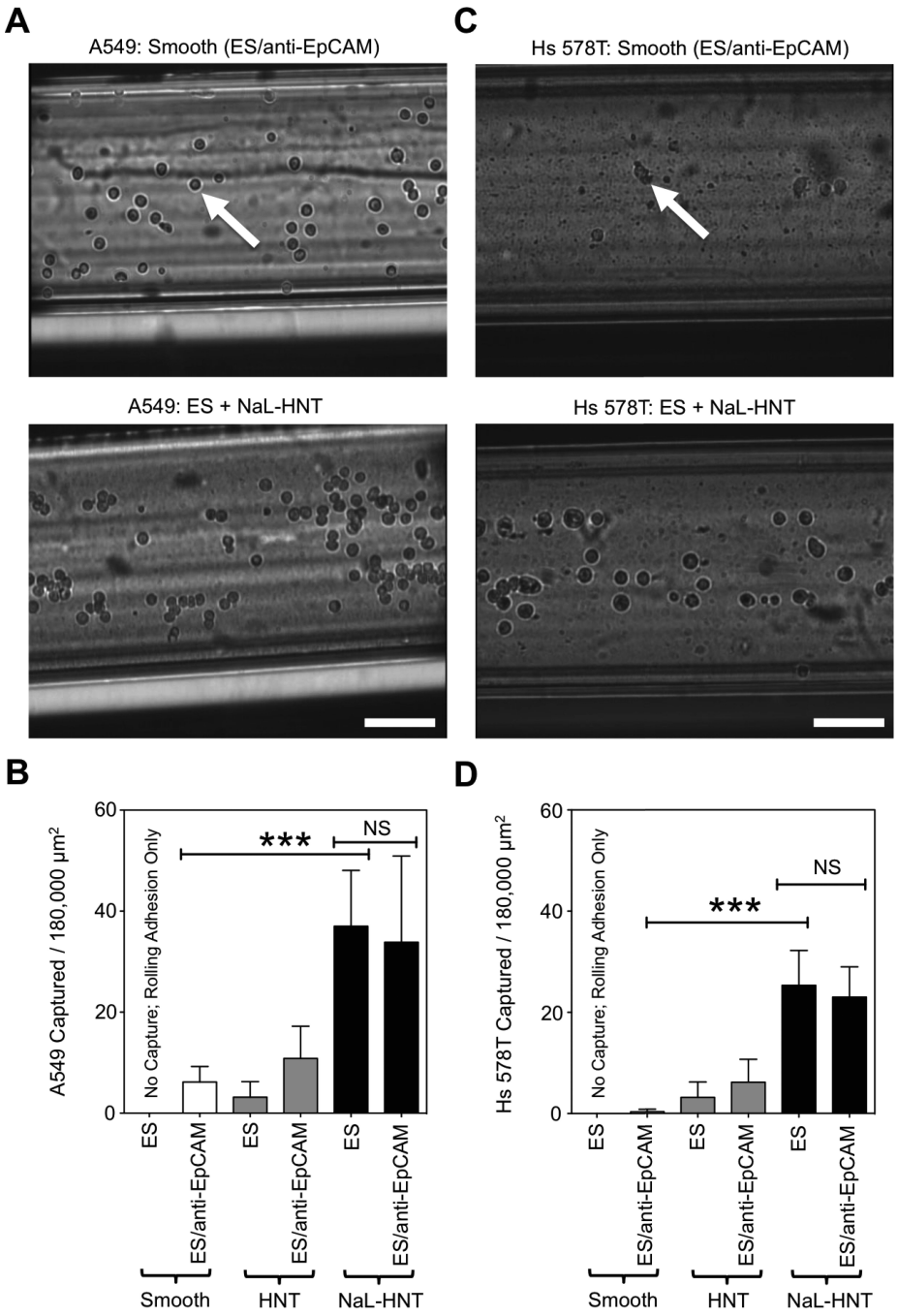

Figure 7.

ES-mediated capture of tumor cells with low to negligible EpCAM surface expression. (A) Representative images of ES-mediated adhesion of A549 tumor cells under flow on smooth surfaces coated with ES and anti-EpCAM antibodies, and immobilized NaL-HNT surfaces coated with ES alone. (B) Number of captured A549 tumor cells per 180,000 μm^2 of biomaterial surface area. (C) Representative images of ES-mediated adhesion of Hs 578T tumor cells under flow on smooth surfaces coated with ES and anti-EpCAM antibodies, and immobilized NaLHNT surfaces coated with ES alone. (D) Number of captured Hs 578T

tumor cells per 180,000 μm^2 of biomaterial surface area. Captured tumor cells denote cells that are firmly adhered to the surface. Calculated values are mean +/− standard deviation. n = 20 or more frames analyzed for captured cells for each condition. Statistics were calculated using a one-way ANOVA with Tukey post test. ***$P < 0.0001$. NS: not significant.

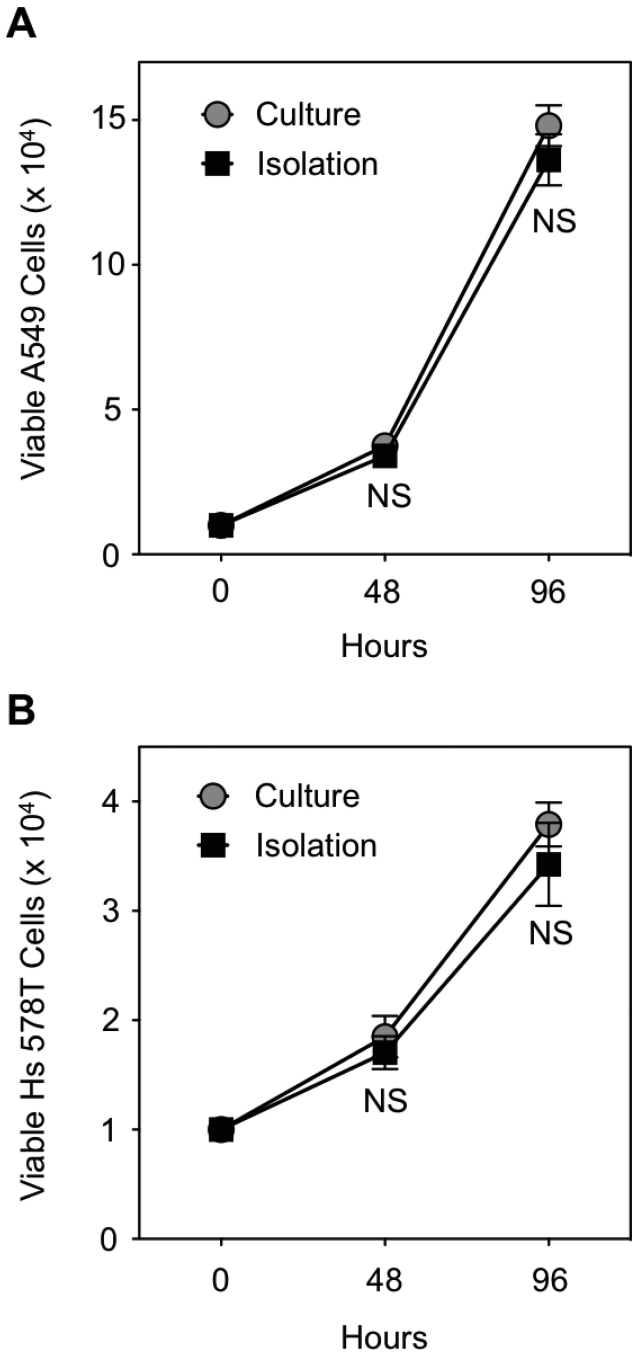

Figure 8.

Growth curves of tumor cells post-isolation from biomaterial surfaces. (A,B) Viable A549 (A) and Hs 578T (B) tumor cells in culture 96 h post-isolation. 10^4 tumor cells isolated from biomaterial surfaces were placed into culture, and growth was tracked for 96 h. Culture: control tumor cell samples harvested from culture. Isolation: tumor cells isolated from biomaterials surfaces and placed into culture. NS: not significant.

Table 1

Zeta potential (in mV) measurements of HNT and NaL-HNT, with and without E-selectin (ES) functionalization, using dynamic light scattering. Data are mean ± standard deviation of three independent measurements.

Sample	Zeta Potential (mV)
HNT	−25.67 +/− 2.55
NaL-HNT	−67.08 +/− 3.94
ES + HNT	−31.57 +/− 2.81
ES + NaL-HNT	−71.21 +/− 4.92

Table 2

Root-mean-square (RMS) roughness measurements of HNT and NaL-HNT using atomic force microscopy. Data are mean ± standard deviation of three independent measurements.

Sample	RMS Roughness (nm)
HNT	163.14 +/− 34.52
NaL-HNT	132.31 +/− 48.47